Numerical Modeling of 3D Printed Electric Machines

Jerry Waterman*, Alexander Clucas†, Timothy B. Costa‡, Yue Zhang† and Julia Zhang†
*Department of Mechanical Engineering
†Department of Electrical Engineering and Computer Science
‡Department of Mathematics
Oregon State University, Corvallis, Oregon 97330

***Abstract*—Additive manufacturing is opening up new ground for innovations in low-volume production due to faster and cheaper prototyping, reduced lead times, and shorter supply chains. As a result, 3D metal printing may present opportunities for electric machine manufacturing. Also, the interest in the research community in determining the quality, reliability, and performance of 3D printed machines is growing dramatically. This paper analyzes the mechanical performance and reliability of an interior permanent magnet synchronous machine, that uses the additive manufacturing process of 3D printed metal.**

I. Introduction

Utilizing an additive manufacturing process to make metal parts for engines and cars, particularly parts with highly complicated structures, is fairly novel. For example, General Electric is using 3D printing to create complex parts with high precision using additive manufacturing processes [1] and United Technologies Research Center is building high power electric machines for automobile traction electric machines and renewable energy generators [2]. Despite the advantages of the additive manufacturing process over traditional methods, concerns exist regarding the reliability and strength of 3D printed objects, as well as regarding the cost and speed for high-volume production. The additive manufacturing process investigated in this paper is the Laser Beam Melting (LBM) process. In LBM, a 3D CAD drawing of a part is sliced into 2D layers, and then the 3D part is built by repeating two main steps. First, a thin layer of metal power is deposited on an initial plate. A laser then follows the 2D slice to melt the powder into a solid material. The build process then repeats these steps moving vertically, melting layer upon layer. Each layer after the first layer partially re-melts the previous layer to create a cohesive bond [3]. This process can create a very complex and heterogeneous micro-structure, as can be seen in Figs. 1 and 2. This work takes a first step towards analysis of the mechanical properties of an electric machine made with the additive manufacturing method through numerical simulations.

The current simulation framework includes: (1) setting up two cohesive behavior interfaces between three layers, (2) building a three layered rotor that rotates about a fixed axis, (3) applying mechanical boundary conditions to understand possible failure modes, and (4) completing the electric machine by adding the electromagnetic solicitations. This paper contains preliminary work describing the rotation of three layers and two cohesive behavior interfaces of the 3D printed rotor, while (3) and (4) will be completed in future work.

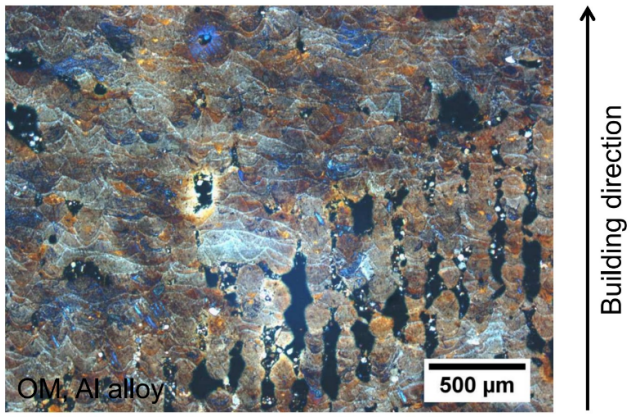

Fig. 1. A scan of a 3D printed aluminum alloy. Notice the distinct layers that are partially melted together to form the solid object. This illustrates the heterogeneous properties of the material. (Figure is cited from [3])

II. Finite Element Modeling

The simulations in this work are performed with the finite element method, which has vast applications in the mathematical, scientific, and engineering communities. The simulations utilize a commercial finite element analysis software Abaqus, which has capabilities for simulating the mechanical as well as the electromagnetic components of this research.

The geometry and size of the electric machine in the simulations are similar to those of the traction electric machine on a Toyota Prius hybrid electric vehicle. The true device is printed in layers approximately 100 μm thick. Thus in an 87mm tall rotor, there are approximately 870 layers of steel. In this work, completion of the simulations of two and three layer devices with one and two bonding regions, respectively, are completed. Only the visual results from the three layered system are included in this report. This is a first step towards simulating the full model.

Mechanical failure of the bonding regions of the simulated electric machine appears mathematically as a discontinuity in the displacement field of the machine under appropriate loads corresponding to rotation. To model this, potential crack surfaces are modeled as interfaces between layers of the simulated model. The model is then completed by defining cohesive behavior surface interaction. This consists of a criteria

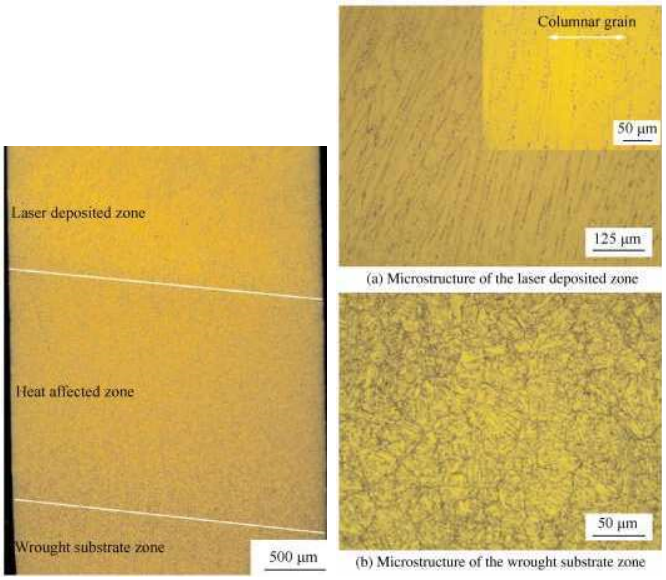

Fig. 2. Micro-structure of hybrid steel (left). Micro-structure layer variances (right). Notice the heterogeneous nature of the laser melted steel, which can cause bonding issues. (Figure is cited from [6])

under which failure will occur. When the criteria is met, a crack propagates along the predefined crack surface.

Using the model of a rotating device with a weakened bonding layer, this methodology is adequate, as it is reasonable to assume that under a uniform load, if a crack occurs, it will occur in the bonding layer. For more complicated, heterogeneous materials, a more robust model of crack initiation and propagation may be necessary. Thus, in future work consideration will be made for a variational model of crack propagation replacing the predefined crack location and cohesive behavior surface interaction definition. This is under the assumption that the material under load will minimize the sum of its surface and volume potential energies [4, 5].

Fig. 2 (right) shows that there is evidence on a microscopic level that the layering is asymmetric and non-uniform. Fig. 2 (left) depicts the layering with the wrought substrate zone on the bottom, the heat affected zone in the middle, and the laser deposited zone on the top. The layers do not show the same consistency in the orientations of the layers of metal, thus lending support to the claim that the 3D printed rotor would be heterogeneous. Recent publications on laser melting deposition of steel at a microscopic level infer a metallurgical bonding between the laser deposited zone and the wrought substrate [6]. Variations between the two layers exist as there is less strength and more elongation in the wrought substrate then the bonding zone of a hybrid fabricated TC11 titanium alloy [7]. These results concern characteristics of the Laser Beam Melting (LBM) process, and they give evidence for the non-uniformity and heterogeneous nature of 3D printed metal.

In this work, the layer non-uniformity at a macroscopic level of a rotor as part of an electric machine is analyzed. A comparison of a model of a 3D printed electric machine with three layers, as shown in Fig. 3, versus a two layered rotor, as shown in Fig. 4, is made. As mentioned above, the size of an individual 3D printed metal layer is 100 μm thick, and in Fig. 3 their thicknesses are generated as 20mm, 10mm, and 5mm. The purpose of this three layered system is to approximate the

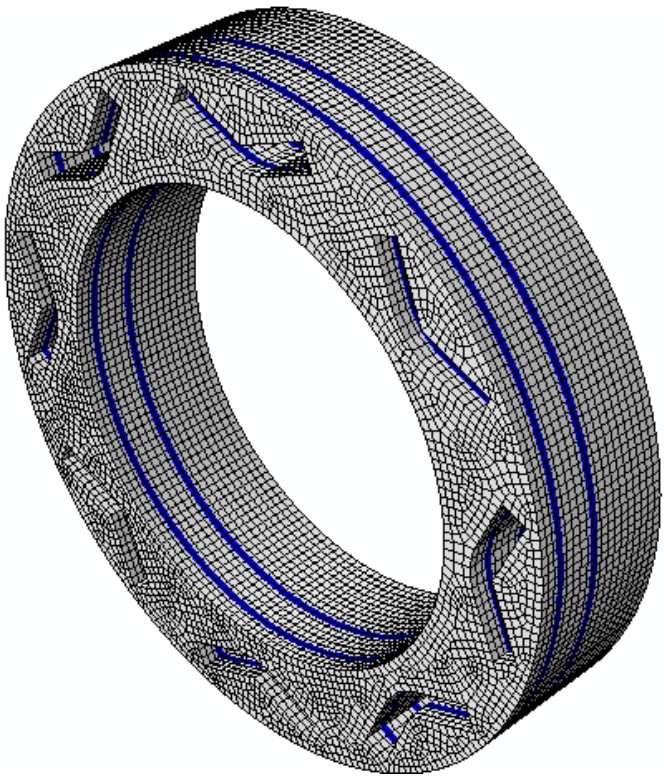

Fig. 3. Fine mesh of the whole section containing three layers and two interfaces.

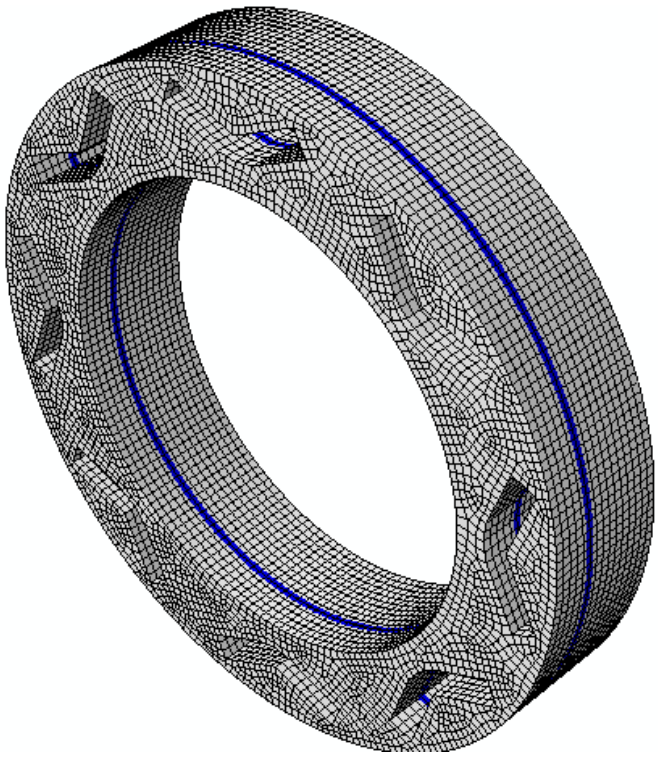

Fig. 4. Fine mesh of the whole section containing two layers and one interface.

complete rotor. This assumes that the rotor is divided into three main sections according in the nonuniform and heterogeneous material. The 3D printed rotor in the simulation uses the material properties of M15 steel for its density and elasticity. The value for the density of the material is $7.56 \cdot 10^{-6} \frac{kg}{mm^3}$ and the value for the elasticity is $2.00 \cdot 10^{5} \frac{N}{mm^2}$. The units are converted from the standard SI units of meters to reflect the geometry dimension in millimeters that is used in this simulation.

The stiffness coefficients that are used for this simulation is assumed to be at 3,000, 3,000, and 3,000. Fig. 5 and Fig. 6 contain stiffness coefficients of 6,000, 6,000, and 6,000. The stiffness coefficients correspond to the normal, shear, and tangential stiffness components respectively. These values for the coefficients are unitless and they describe the degree to which the layers are bonded to each other. The reason for why it is determined to set these coefficients as different from each other is to contribute the heterogeneous nature of the simulation. The coefficients are assumed values and do not necessarily reflect reality. In the validation stage of the research, the goal will be to obtain the correct values for the coefficients.

Figs. 5 and 6 illustrate two increments of time in the simulation and how the damage on the first interface between layers 1 and 2 is distributed on the geometry of the rotor. Figs. 7 and 8 also contain two increments of time, they analyze the second interface in the three layered simulation. The legend on Figs. 5 to 8 correspond to values ranging from 0.00 to 1.00, which corresponds to 0% damage and 100% damage respectively. At 0% the interface as taken no damage and is not being debonded. At 100% the interface has taken complete damage and is fully debonded. The legends of Figs. 5 to 8 have status variables for their numerical values.

The damage percentages of Figs. 5 to 8 are calculated based on the Traction-Separation law that is defined in the interaction properties in Abaqus Explicit. The criterion for the initiation of damage is the maximum nominal stress with 11, 5, and 5 as the mode 1, mode 2, and mode 3 values respectively. The damage evolution law describes the rate at which the cohesive surfaces is degraded once the corresponding initiation criterion is reached. A linear softening law is chosen to define the detailed evolution between the damage initiation and complete failure.

The simulation from beginning to end is run from 0.00 to 0.80 seconds. Data is generated at increments in time of 0.05 seconds for a total amount of valid increments of 16. The simulation ends at 0.80 seconds due to the bonds of both of the interfaces being destroyed. The general trend seen here is that the damage spreads from the center and spreads to the outer circumference. Figs. 7 and 8 accrue damage slower than Figs. 5 and 6 making it take longer to fully debond. The differences in these two interfaces are due to the different thicknesses that were set in layers 1 and 2 as compared to 2 and 3, also because of the differences in the values for the given stiffness coefficients.

This simulation is created by using the following general steps in the finite element analysis tool Abaqus Explicit:

1) Creating geometry with solid extrusions of the layers then assigning the material properties of steel to those solids
2) Generating a mesh using the automatic feature of the

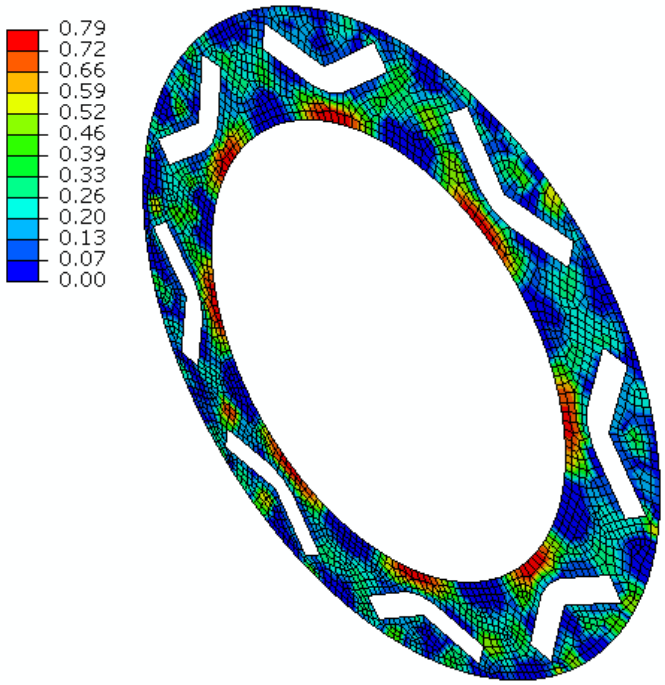

Fig. 5. Visual representation of the first interface of the simulation between layers 1 and 2. This image occurred after 0.20 seconds. At this stage the cohesive behavior of the interaction is taking damage on the surface of the interface meaning that the layers are debonding.

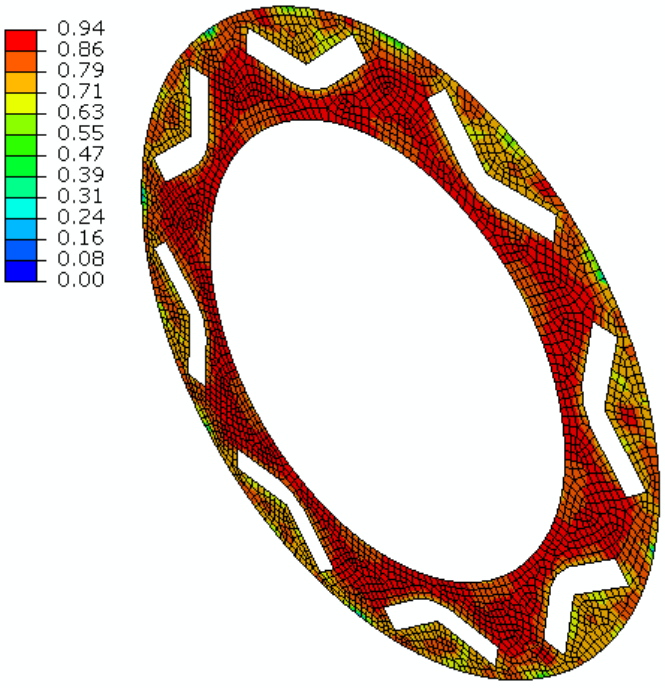

Fig. 6. Visual representation of the first interface of the simulation between layers 1 and 2. This image occurred after 0.30 seconds. At this stage the cohesive behavior of the interaction has taken a great deal more damage throughout than in Fig. 5.

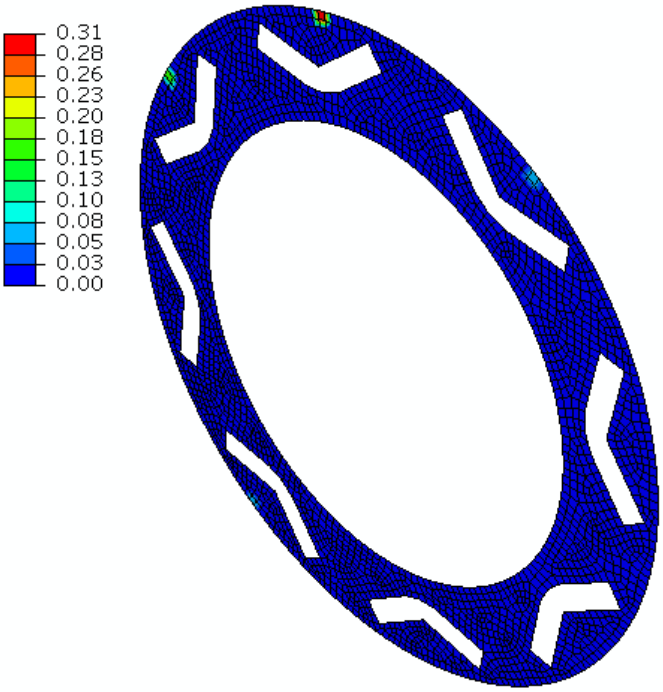

Fig. 7. Visual representation of the second interface of the simulation between layers 2 and 3. This image occurs after 0.20 seconds. At this stage the cohesive behavior of the interaction has taken minor damage on small patches of the outer circumference meaning that the layers remain mostly bonded together.

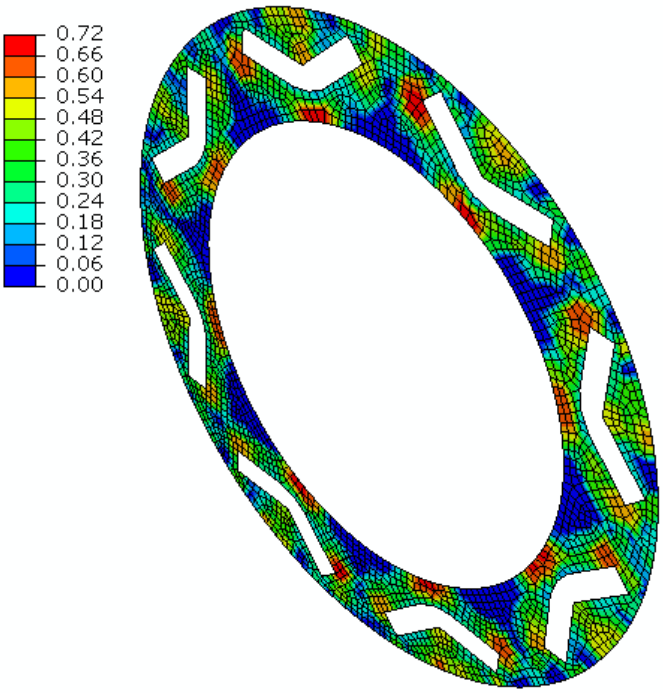

Fig. 8. Visual representation of the second interface of the simulation between layers 2 and 3. This image occurs after 0.30 seconds. At this stage the cohesive behavior of the interaction has taken moderately more damage than shown in Fig. 7.

finite element software after setting global seeds of 2mm

3) Defining the geometry as a rigid body constrained about reference points for each of the three layers
4) Setting boundary conditions to the reference points to rotate at an angular velocity of 300 rad/s
5) Defining a master and slave cohesive behavior interaction between the first and second layer, and the second and third layer
6) Assigning the three solid layers as instances and using position constraints for them to be face to face and concentric
7) Submitting the job to generate data and observe the graphical results through visualization

The overall purpose of the simulation is to determine if a 3D printed steel rotor's cohesive behavior between layers could withstand the rotational forces that a rotor undergoes in an electric machine. Given a max rotational velocity of 15,000 RPM, that would be equivalent to approximately 1,600 rad/s which is needed as a minimum requirement. The rotational velocity that is used for the 3 layered simulation is 300 rad/s as a base point for observation of the results. Future simulations will include different values for the set angular velocity of the rigid bodies.

To verify that the results from the simplified model represents reality, experimental verification will be performed on 3D printed metal bars. The experiments will be performed on bars of dimension $100.0 \times 15.0 \times 3.0$ millimeters, in three materials: AlSi10Mg Aluminum, Ti64 Titanium, and PH1 Stainless Steel. Three standard tests will be performed: a tensile test, a compression test, and a three point bending test. The results from the physical experiment can then be compared to the results generated with the finite element analysis simulations.

A tensile test involves slowly extending a specimen until it fractures, resulting in a mode I crack. As the material is extended, the elongation is recorded against the applied force. These values are non-dimensional and a stress-strain curve is produced. A compression test is similar to a tensile test, except that the material is compressed rather than elongated. This will eventually produce a buckling in the material as it deforms.

The three point bending test is performed by setting the ends of the test material on two supporting pins, while a third loading pin is lowered at a constant rate from above a point in-between the two supporting pins until the material fails. This process results in a mode I crack.

These standard tests will verify that the simplified FEA model responds similarly to true 3D printed materials under a variety of loads. However, these tests do not represent the load type these simulations are utilizing to verify the integrity of a 3D printed electric machine. For this purpose, a fourth test will be performed in which the material is clamped on one end and a rotational force is applied to the other end of the rod. This will result in a mode III crack, similar to the type expected for the simulated FEA model.

In Fig. 9 the damage over the time and angular velocity of the rigid body over the damage of the first interface is plotted. An interface is defined as the cohesive behavior interaction set between the master and slave condition of two respective adjacent layers. Fig. 10 indicates that the first cohesive behavior interface does not undergo damage until

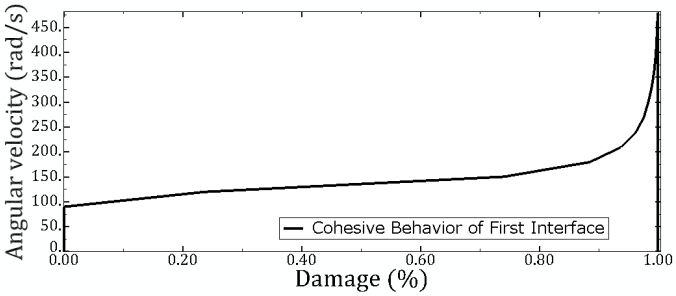

Fig. 9. Angular velocity of the rigid body over damage of the first interface.

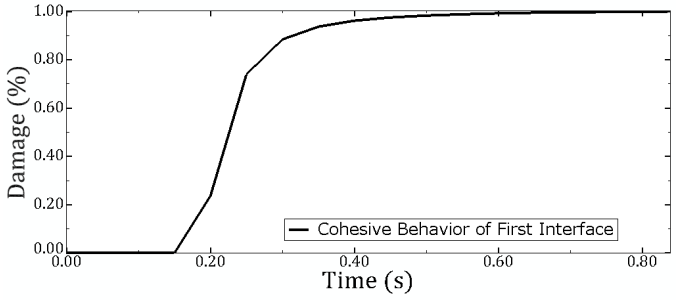

Fig. 10. Damage of the first interface over time.

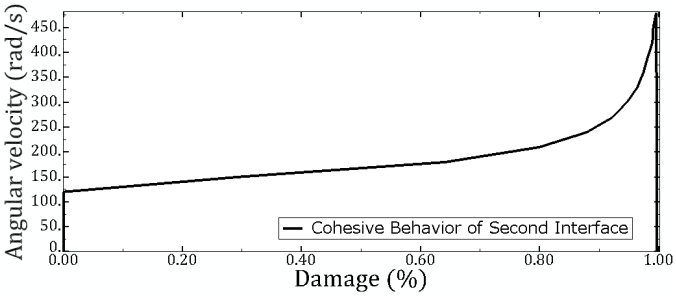

Fig. 11. Angular velocity of the rigid body over damage of the second interface.

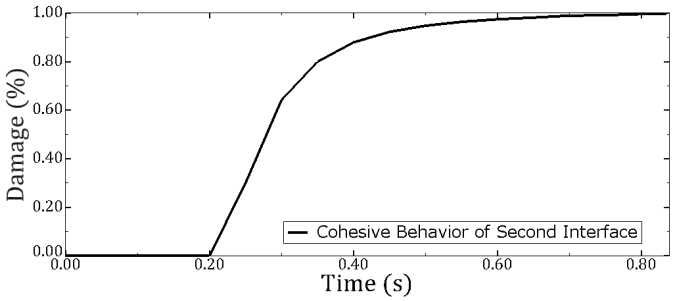

Fig. 12. Damage of the second interface over time.

approximately 0.15 seconds, upon which it sharply increased in damage. This process continues and then begins to level off at time equals 0.25 seconds as the interface approaches complete destruction. Fig. 9 shows that the first interface does not begin being damaged until it reaches the angular velocity of approximately 90 rad/s. This value is significantly below the minimum angular velocity requirement of 1,600 rad/s.

Figs. 11 and 12 utilize the same plotting methods as Figs. 9 and 10, applied to the second and third layer as the second interface. Fig. 12 indicates that the first cohesive behavior interface does not undergo damage until approximately 0.20 seconds, upon which it sharply increased in damage. This process continued and then begins to level off at time equals 0.35 seconds as the interface approached complete destruction. Fig. 11 shows that the second interface does not begin being damaged until it reached the angular velocity of approximately 130 rad/s. This value is an improvement over the results of the first simulation, but is still significantly below the minimum angular velocity requirement of 1,600 rad/s.

Under the assumption that the thicknesses and the cohesive behavior coefficients are an accurate representation of reality, the graphs indicate overall that the 3D metal printed rotor does not have the required mechanical properties needed to withstand the forces that are experienced in operating an electric machine. By going through with the physical experiments testing the 3D printed metal materials, correct coefficients can be determined which would aid in the accuracy and reliability of the simulations.

III. Conclusions

This research is aimed at modeling the functionality of electric machines created using additive manufacturing processes. The integrity of these machines is imperative to the safety of the operations they perform. Using a mechanical model, it is expected that the layers would shear from each other by weakening the bonding strength.

Plots are generated of the damage in the simulations as seen in Figs. 9 to 12. This gives a pattern for how the interfaces between the layers are destroyed. Based on the assumed thicknesses and coefficients, both of the interfaces began to take damage at angular velocities of less than 150 rad/s. This therefore means that if the assumed values used in the simulation are accurate, the mechanical properties of a 3D printed rotor are not sufficient for high speed operation.

This work represents a first step towards robust simulations of mechanical integrity of 3D printed electric machines. For visual verification, the layers are simulated thicker than those present in a true 3D printed device. In addition, this work simulates simplified structures with two and three layers, corresponding to one and two bonding regions, respectively. Finally, the assumption is that any crack will propagate exactly along the bonding interface between layers.

In future work, these simplifications will be addressed by simulating true layer thicknesses, and including many layers connected by bonding regions. Additionally, considerations for models that allow for crack propagation along unpredictable surfaces will be made. The electromagnetic model will include determining if there are significant differences in the core loss due to the layering of the rotor and stator.

References

[1] J. Lucas, NineSigma, GE Names 10 Finalists in GE Global 3D Printing Production Quest, *Professional Services close-Up Business Insights: Global*, **(2015)**.

[2] B. Wilson and W. Veronesi, Additive manufacturing of optimized ultra-high efficiency electric machines, *Connecticut Center for Advanced Technology* **(2013)**.

[3] A. Mertens, Additive Manufacturing of Metal Materials: Case Studies in the Processing of Stainless Steel 316L and of Alloy Ti-6Al-4V by Laser Beam Melting, *Universityé de Liège.* **(2014)**.

[4] B. Bourdin, G. A. Francfort, and J.-J. Marigo, The Variational Approach to Fracture, *J. Elasticity*, **(2008)**.

[5] G. A. Francfort and J.-J. Marigo, Revisiting Brittle Fracture as an Energy Minimization Problem, *J. Mech. Phys. Solids.*, **(1998)**.

[6] Y. Wang, H. Tang, Y. Fang, and H. Wang, Micro-structure and mechanical properties of hybrid fabricated lCrl2Ni2WMoVNb steel by laser melting deposition, *Materials Science and Engineering* **(2013)**.

[7] Y. Zhu, J. Li, X. Tian, H. Wang, and D. Liu, Micro-structure and mechanical properties of hybrid fabricated Ti-6.5Al-3.5Mo-1.5Zr-0.3Si titanium alloy by laser additive manufacturing, *Materials Science and Engineering*, **(2014)**.